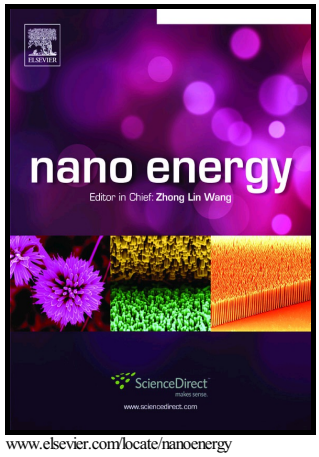

www.elsevier.com/locate/nanoenergy

The effect of interfacial pH on the surface atomic elemental distribution and on the catalytic reactivity of shape-selected bimetallic nanoparticles towards oxygen reduction

Rosa M. Arán-Ais, José Solla-Gullón, Martin Gocyla, Marc Heggen, Rafal E. Dunin-Borkowski, Peter Strasser, Enrique Herrero, Juan M. Feliu

PII: S2211-2855(16)30264-6
DOI: http://dx.doi.org/10.1016/j.nanoen.2016.07.024
Reference: NANOEN1399

To appear in: *Nano Energy*

Received date: 14 April 2016
Revised date: 15 July 2016
Accepted date: 22 July 2016

Cite this article as: Rosa M. Arán-Ais, José Solla-Gullón, Martin Gocyla, Mar Heggen, Rafal E. Dunin-Borkowski, Peter Strasser, Enrique Herrero and Jua M. Feliu, The effect of interfacial pH on the surface atomic elemental distributio and on the catalytic reactivity of shape-selected bimetallic nanoparticles toward oxygen reduction, *Nano Energy,* http://dx.doi.org/10.1016/j.nanoen.2016.07.024

The effect of interfacial pH on the surface atomic elemental distribution and on the catalytic reactivity of shape-selected bimetallic nanoparticles towards oxygen reduction

Rosa M. Arán-Ais[1], José Solla-Gullón[1], Martin Gocyla[2], Marc Heggen[2], Rafal E. Dunin-Borkowski[2], Peter Strasser[3], Enrique Herrero[1], Juan M. Feliu[1,*]

[1]Instituto de Electroquímica, Universidad de Alicante, Apdo. 99, E-03080 Alicante, Spain

[2]Ernst Ruska-Centre for Microscopy and Spectroscopy with Electrons, Forschungszentrum Jülich GmbH, 52425 Jülich, Germany.

[3]The Electrochemical Energy, Catalysis, and Materials Science Laboratory, Department of Chemistry, Chemical Engineering Division, Technical University Berlin, 10623 Berlin, Germany.

[*]Corresponding author: juan.feliu@ua.es

Graphical Abstract

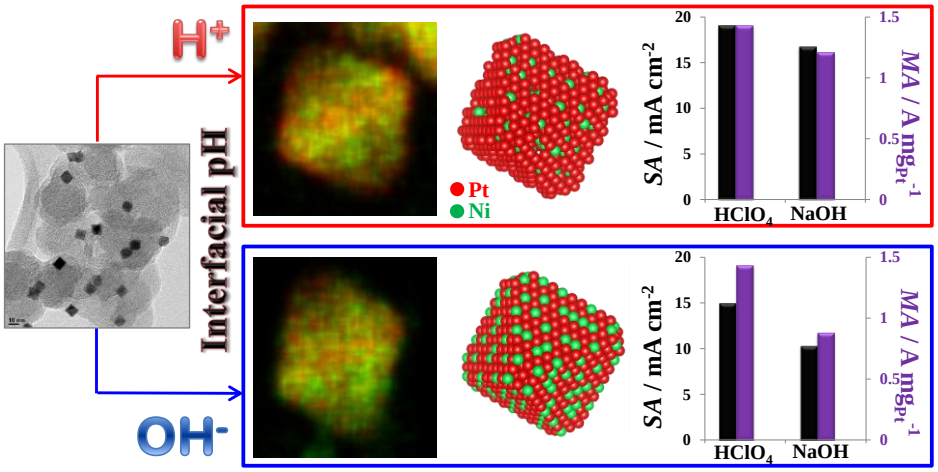

Abstract

The effect of interfacial pH during the surface cleaning of shape-selected PtNi nanoparticles was investigated. High-angle annular dark field (HAADF) scanning transmission electron microscopy (STEM) and energy-dispersive X-ray (EDX) elemental mapping techniques were used to analyze the morphology and composition of the particles at the nanoscale. The particles show similar atomic compositions for both treated samples but different elemental distribution on the surface of the nanooctahedra. X-ray photoelectron spectroscopy (XPS) analysis confirmed different surface compositions and the presence of different oxidation states species at the outer part of the nanoparticles. In addition, we compare characteristic voltammetric profiles of these nanocatalysts when immersed in three different aqueous supporting electrolytes (H_2SO_4, $HClO_4$ and NaOH). The behavior of the bimetallic nanoparticles towards adsorbed CO oxidation has been analyzed and compared with that observed after surface disordering of the same catalysts. The electrocatalytic activity of these nanoparticles has been also tested for the electroreduction of oxygen showing high specific and mass activity and better catalytic performance than pure Pt shaped nanoparticles. The different treatments applied to the surface of the nanocatalysts have led to remarkably different catalytic responses, pointing out the

outstanding importance of the control of the surface of the alloyed shape-selected nanoparticles after their synthesis and before their use as electrocatalysts.

Keywords: Interfacial pH, PtNi octahedra, Surface cleaning, Surface composition, Electrocatalysis, Oxygen reduction reaction.

1. Introduction

Low temperature fuel cell technology has been extensively studied over the past few decades due to its promise for applications in transportation, stationary and portable power generation [1, 2]. To achieve a wider deployment of these devices, several technical challenges must be addressed, namely high cost (platinum (Pt) is the most used catalyst, principally at the cathode), low durability (due to dissolution problems) and substantial overpotential for the electroreduction of oxygen [3, 4]. In this sense, it has been demonstrated that alloying Pt with other transition metals produces cheaper electrocatalysts with novel properties for the oxygen reduction reaction (ORR) due to lattice compression [5, 6] and/or concomitant modified electronic properties [7, 8]. To these ends, full extended bimetallic Pt surfaces have been studied, showing greatly enhanced activities for the ORR [7, 9]. In particular, Pt_3Ni [10, 11], Pt_3Co [12], Pt_3Fe [9], and Pt alloyed with early transition metals like Pt_3Sc, Pt_5Ga and Pt_3Y [13-17] have all exhibited higher activity than pure extended Pt surfaces. These results have been translated to alloyed nanoparticles [15, 18-23]. Besides the composition, the size and the shape of the nanoparticles play a critical role for their electrocatalytic activity. The ORR activity results from a convolution of the proportion of active sites in the surface terraces of the nanoparticles and a maximum in mass activity as the particle size decreases [21, 24]. In addition, ORR is known to be very sensitive to the surface structure of the heterogeneous interface where it takes place [10, 25-27], since the different atomic arrangement influences the adsorption of the reactant species onto the surface during the reaction. Thus, by synthesizing

nanoparticles with a particular shape it is possible to control their atomic surface structure and, therefore, developing novel catalysts with higher activity and selectivity. Special interest has attracted the synthesis of octahedral PtNi nanocatalyst, since they were revealed as ideal catalysts for the ORR [28]. The best activity reported so far for 9 nm PtNi octahedral nanoparticles was reported by Choi et al. [29]. These electrocatalysts were obtained by using the mixture oleylamine (OAm)/oleic acid (OA) in the presence of benzyl ether (BE) and using $W(CO)_6$ as reducing agent.

Critical to the final catalytic activity is the nature of the post-synthesis treatment prior to catalyst use. In many reports, a post-treatment in heated acidic media is necessary to remove any remaining capping agents from the synthesis, producing a partial or total leaching of the non-noble metal from the surface of the nanoparticles and leading to a skeleton-type structure [12]. In this sense, Stamenkovic et al. [9] showed that, in the case of Pt skeleton crystal surfaces, Pt_3Co and Pt_3Ni are at the top of the ORR volcano. Open structures consisting of Pt_3Ni nanoframes have been addressed by preferential removal of Ni from the facets of solid Ni rich polyhedra, followed by an annealing process that leads to highly crystalline hollow Pt-skin nanostructures that set the activity benchmark for ORR [30]. These results point out that, besides the control over the shape and composition of the nanocatalysts during synthesis step, any post-treatment applied to the as-prepared materials strongly affects their final surface structure and composition, and thus the electrocatalytic activity. In this regard, the understanding of the interfacial properties is a challenging topic in electrocatalysis that requires precise experiments combining different techniques.

The mixture OAm/OA has been widely used over the last few years as surfactant, solvent and reducing agent to obtain high quality Pt and Pt-based alloy nanocrystals with different sizes and shapes [29-35]. Recently, a new decontamination protocol for nanoparticles synthesized by this method has been developed [36]. It was demonstrated for Pt nanoparticles that this method effectively removes any remaining surfactants while preserving the surface structure of the nanoparticles. It is expected that, since this cleaning method does not apply any acidic

treatment, the non-noble metals would not be removed and the composition on the surface would remain the same as it was post-synthesis, also preserving its well-ordered surface structure in the case of shaped nanoparticles.

In this work we aim to understand the changes in surface atomic elemental distribution, morphology and composition induced by post-synthesis treatments in vastly different pH environments. Such pre(catalysis)treatments are required for an effective removal of the remaining capping agents and the resulting effect on the electrocatalytic activity for ORR. To achieve this, this study combines microscopic, spectroscopic and electrochemical measurements on octahedral PtNi nanoparticles with different surface composition. In particular we study post-synthesis treatments at opposite pH: (1) acid treatment, i.e. chemical leaching of the Ni at the surface, leading to a skeleton-type structure, and (2) alkali treatment, precluding the dissolution of either Pt or Ni. The study here presented demonstrates that the composition of the interphase nanoparticle surface | solution can be significantly different from that of the bulk nanocatalyst. The different cleaning protocols applied to the surface of the bimetallic octahedra have shown that the species present at the nanoparticles' surface are pH-dependent, leading to interestingly different catalytic responses, and pointing out that the way they are decontaminated drastically affect their performance as electrocatalysts.

2. Material and Methods

2.1. Reagents

Platinum(II) acetylacetonate ($Pt(acac)_2$, 97%), nickel(II) acetylacetonate ($Ni(acac)_2$, 95%), oleylamine (OAm, 70%), oleic acid (OA, 90%), benzyl ether (BE, 98%) and tungsten hexacarbonyl ($W(CO)_6$, 99.99%) were purchased from Sigma-Aldrich. Acetic acid (HAc, 96%), sodium hydroxide (NaOH, p.a.) and 2-propanol (Reag. Ph. Eur) were obtained from Merck. Methanol, ethanol and acetone (Reag. Ph. Eur) were purchased from Panreac, and n-hexane (96%) from Scharlau. All the chemicals were used as received without further purification.

2.2. Material Characterization

Transmission electron microscopy (TEM) measurements were performed with a JEOL JEM-2010 microscope working at 200 kV and with a JEOL JEM-1400 Plus working at 120 kV. The samples were prepared by placing a drop of the hexane suspension onto a Formvar-covered copper grid and drying it in air at room temperature. For each sample, usually about 200–300 particles from different parts of the grid were used to estimate the mean diameter and size distribution of the nanoparticles.

Scanning transmission electron microscopy (STEM) was performed using an FEI Titan 80-200 ("ChemiSTEM") electron microscope operated at 200 kV, equipped with a Cs-probe corrector (CEOS GmbH) and high-angle annular dark field (HAADF) detector. In order to achieve "Z-Contrast" conditions a probe semi-angle of 25 mrad and an inner collection semi-angle of the detector of 88 mrad were used. Compositional maps were obtained with energy dispersive X-ray (EDX) using four symmetric large-solid-angle silicon drift detectors. For EDX measurement, an FEI double-tilt holder was used and the TEM specimen was untilted. EDX maps were extracted using the Pt L and Ni K lines and the ESPRIT software (Bruker Company, Berlin, Germany). The 1 σ statistical error in the EDX quantification of ± 2 at. %, is dominated by the counting statistics. For all samples at least 10 high resolution EDX maps of different nanoparticles were obtained.

Inductively coupled plasma mass spectroscopy (ICP-MS) was used to determine the atomic composition of the different catalysts, using the Agilent 7700x analysis system. The samples were prepared by dissolving the catalysts powders in aqua regia (3 HCl:1 HNO_3). The solutions were heated from room temperature to 200 °C in 10 min using a Microwave Discover SP-D (CEM corporation), keeping at this temperature during 20 min. Finally, the cooled solutions were diluted with MilliQ water, filtered and taken to a known volume.

X-ray photoelectron spectroscopy (XPS) measurements were recorded on a KAlpha Thermo Scientific spectrometer using AlKα (1486.6 eV) radiation, monochromatized by a twin crystal

monochromator and yielding a focused X-ray spot with a diameter of 400 μm, at 3 mA × 12 kV. Deconvolution of the XPS spectra was carried out using a Shirley background.

2.3. Synthesis of octahedral PtNi nanoparticles

The nanoparticles were prepared using a similar method to that described by Choi et al. [29], but being scaled up by a factor of 5 in order to obtain much more product. In brief, 0.255 mmol $Pt(acac)_2$, 0.195 mmol $Ni(acac)_2$, 10.0 mL OAm, 5.0 mL OA and 35.0 mL BE were loaded into a three-neck flask equipped with a condenser. The mixture was heated to 130 ºC with magnetic stirring under argon purging. Once the homogeneous solution reached this temperature, 0.710 mmol $W(CO)_6$ was rapidly added and the argon stream was stopped. The temperature was subsequently raised to 230 ºC (heating rate of 10 ºC min^{-1}, approximately) and then maintained for 40 min. The resulting solution was allowed to cool down naturally and the product was isolated by centrifugation (6000 rpm, 10 min). The PtNi octahedra were washed once with a mixture hexane/ethanol (1:1) and finally dispersed in a known volume of hexane.

2.4. Preparation of PtNi/C catalysts

The suspension of PtNi octahedra in hexane was added to a solution of carbon (Vulcan XC72R) in hexane. The mixture was intermittently stirred and ultrasonicated at room temperature (RT) for 3 h, and aged overnight. The resulting solution of PtNi/C catalyst was divided in two parts in order to apply two different washing protocols.

2.5. Acid-treated PtNi/C catalysts

One portion of the suspension of PtNi/C in hexane catalyst was precipitated by adding ethanol and further centrifugation. The resulting solid was dispersed in 40.0 mL of acetic acid and heated to 60 ºC for 6 h under magnetic stirring. The final catalyst was washed 3 times with ethanol, filtered and dried for 30 min in an oven at 70 ºC.

2.6. Alkaline-treated PtNi/C catalysts

The other portion of the PtNi/C suspension was also precipitated by adding ethanol and further centrifugation. The resulting supported nanoparticles were washed following the method described in a previous work [36], which has been demonstrated to effectively remove the capping agents OAm/OA from the nanoparticles without perturbing their surface structure. Briefly, the precipitate was dispersed in 40.0 mL of methanol and 2 pellets of NaOH (about 0.4 g) were added to the dispersion, which was sonicated for 5 minutes. The supported nanoparticles were allowed to naturally precipitate overnight. Then, the alkaline solution of methanol was removed and the particles were washed with acetone. This procedure methanol+NaOH/acetone was repeated three times. Finally, the catalyst was washed 3 times with ethanol, filtered and dried for 30 min in an oven at 70 ºC.

Scheme 1 illustrates the synthetic steps toward the pH treated shape-selected PtNi nanoparticles:

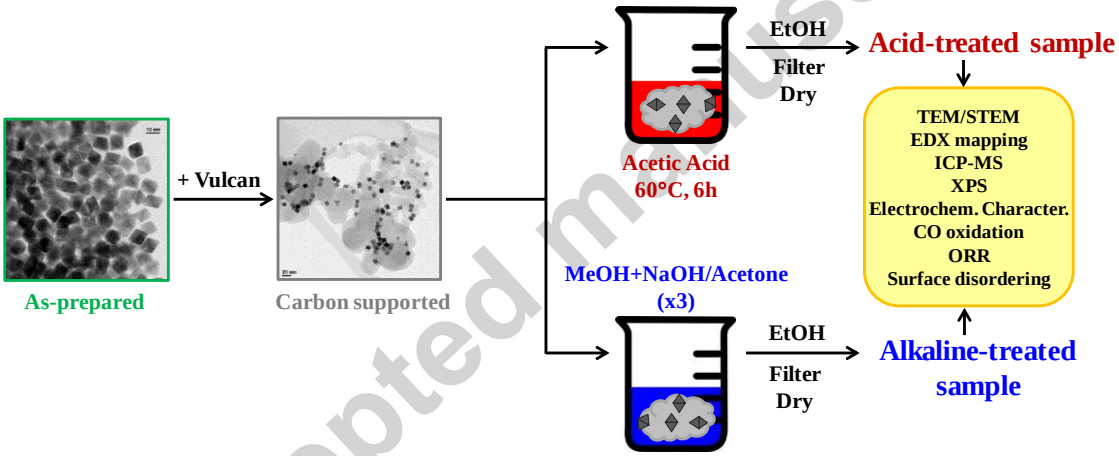

Scheme 1. Scheme of the preparation of the different PtNi/C samples and the different techniques used in their morphological, compositional, electrochemical and eletrocatalytic characterization.

2.7. Electrochemical measurements.

A conventional three-electrode cell was used to perform the electrochemical measurements. The counter electrode was a platinum wire and the potentials were measured against a reversible hydrogen (Air Liquide, N50) electrode (RHE) connected to the cell through a Luggin capillary.

The working electrode was prepared by dropping an aliquot of the catalyst ink onto a glassy-carbon (GC) EDI101 Rotating Disk Electrode (RDE) (diameter: 3 mm, geometric area: 0.0707 cm^2) with a CTV101 speed control unit (Radiometer). The electrode rotation rates (ω) were selected between 360 and 4600 rpm. The methodology followed in order to obtain reproducible deposits of catalyst has been described elsewhere [37]. The ink was prepared by dispersing the obtained catalysts in 3.98 mL of MilliQ water, 1 mL of isopropanol and 20 μL of Nafion® 5% wt, and further ultrasonication for 15 min. The Pt loading of the different catalysts tested on the glassy carbon disk were about 7 μg cm^{-2}_{disk}. The electrochemical characterization of the different catalysts by cyclic voltammetry at the sweep rate of 50 mV s^{-1} was performed at room temperature in a Ar (Air Liquide, N50) saturated 0.5 M H_2SO_4 (96%, Merck, Suprapur®), 0.1 M $HClO_4$ (70%, Merck, Suprapur®) and 0.1 M NaOH (99.99%, Merck, Suprapur®) solutions. The electrochemical active surface area (ECSA) was determined by integrating the charge involved in the so-called hydrogen under potential deposition (H_{UPD}) region in the voltammograms obtained in sulfuric acid, assuming 210 μC cm^{-2} for the total charge after the subtraction of the double layer contribution. CO oxidation experiments were carried out by bubbling CO (g) (N47, Air Liquide) through the electrolyte at 0.1 V until complete blockage of the surface, which was monitored by cycling the electrode between 0.05 and 0.3 V. After that, CO was removed from the solution by bubbling Ar for at least 20 min and CO-stripping voltammograms were performed at 20 mV s^{-1} in order to oxidize the CO molecules adsorbed on the surface in a single sweep. ORR measurements were conducted in O_2-saturated 0.1 M $HClO_4$ and 0.1 M NaOH solutions by sweeping the potential from 0.05 to 1.05 V at the scan rate of 10 mV/s and a rotation speed of 1600 rpm. ORR polarization curves were normalized to the substrate's area (0.0707 cm^2). The kinetic currents i_k at 0.9 V were calculated from the ORR polarization curves by considering the Koutecky-Levich equation:

$$\frac{1}{i} = \frac{1}{i_k} + \frac{1}{i_d} \rightarrow i_k = \frac{i_d \cdot i}{i_d - i}$$

where i is the current measured at 0.9 V, i_k is the kinetic current and i_d is the diffusion-limiting current. The electrode potential was controlled using a PGSTAT30 (Metrohm Autolab B. V.) system and a VMP3 multichannel potentiostat (BioLogic) with an NStat configuration (1 counter electrode, 1 reference electrode and 8 working electrodes working simultaneously).

3. Results and Discussion

3.1. Structural and Compositional Characterization.

Figures 1A and 1D show representative TEM and STEM images, respectively, of the as-prepared PtNi nanoparticles, which clearly present an octahedral-like morphology with an average size (estimated by the longest length connecting two opposite vertices) of 13.2 ± 1.1 nm. Most particles have an octahedral shape but occasionally triangles and spherical nanoparticles are found. The size of the obtained nanoparticles is bigger than that expected from previous literature [29]; the scaled up and differences in the temperature rate of the synthesis may be the responsible for this mismatch. Figures 1B & 1E, and 1C & 1F display the carbon supported PtNi nanoparticles after acid and alkaline cleaning treatment, respectively. Both samples exhibit a good distribution of the catalyst on the carbon support, although the nanoparticles treated under alkaline conditions seem to be more agglomerated.

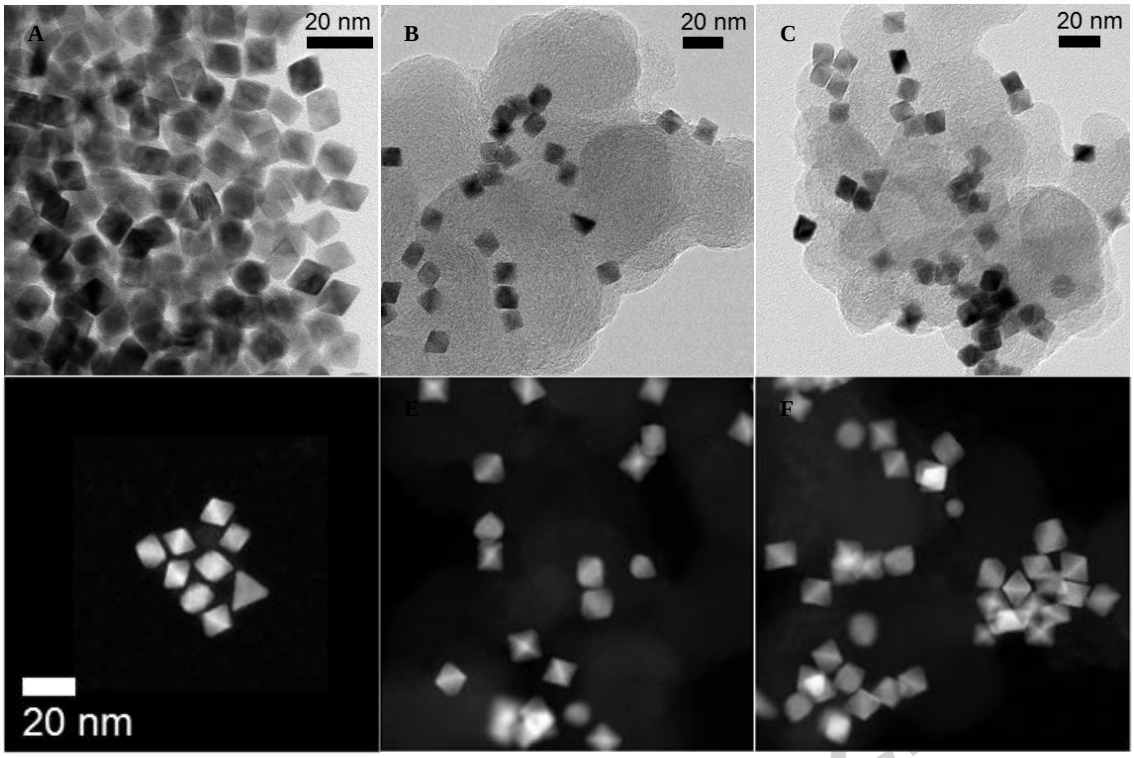

Fig 1. TEM and HAADF-STEM images of Pt-Ni octahedra: as-prepared unsupported nanoparticles (A, D), carbon supported acid-treated nanoparticles (B, E) and carbon supported alkaline-treated nanoparticles (C, F).

In order to get information on the elemental distribution in the as-prepared nanoparticles and the samples treated in different liquid extreme pH environments we performed HAADF-STEM imaging and compositional EDX spectroscopy analysis (figure 2). The HAADF-STEM image of a representative octahedral nanoparticle in its initial state, oriented close to the ⟨110⟩ zone axis can be seen in figure 2A. Dark regions indicate reduced specimen thickness or enrichment in the lighter element at comparable thickness. The EDX maps (figures 2B-D) corroborate this, indicating an enrichment of Ni at the {111} facets and a Pt-rich frame, which is pointed out by a Pt-rich stripe in the middle of the nanoparticles (figure 2B). At the outermost parts of the octahedron a Pt-rich stripe is seen in the EDX images, which coincides with a bright stripe in the HAADF-STEM image (figures 2A and 2B, highlighted by arrows in figure 2A) and is due to the presence of Pt-rich edges or the formation of a thin Pt-rich skin on the facets of the

octahedron. This elemental distribution is in good agreement to earlier works [23, 38, 39]. The corners of the octahedron are slightly rounded. Rounded corners present an energetically more stable shape than sharp edges due to a lowered surface energy[40]. Furthermore, Ni is located at the surface of the particles as well as between neighboring particles (figure 2B, highlighted by an arrow). EDX quantification yields an average composition of Pt 64 at.% and Ni 36 at.%, calculated from the mean value of the atomic composition of ten nanoparticles similar to the nanoparticle imaged in figure 2A.

After acid treatment, the bright stripe at the outermost part is still visible. The particle corners, however, become more rounded (figure 1E). To highlight the effect of edge rounding we fitted circles at a corner and measured the diameter of the circles (figure S1). While the diameter of the as-prepared octahedra is around 1.7 nm, the diameter increases for the acid-treated octahedra up to 4.1 nm. The EDX composition map in figure 2F indicates an elemental distribution which is similar to the initial octahedra, but in some cases a more pronounced Pt-rich skin is found. Interestingly, no Ni is observed between the particles. The reason for the formation of a more pronounced Pt-rich skin could be a combination of the migration of the Pt surface atoms from the corners and the Ni being leached away by the acid from the surface of the octahedra. EDX quantification yields a mean composition of Pt 65 at.% and Ni 35 at.% for nanoparticles as the one imaged in figure 2E, which indicates a minor impact of Ni leaching to the bulk composition of the nanoparticles. Taking only the composition close to the edge of the nanoparticles into account, the acid treated nanoparticles show a composition of about Pt 75 at.% and Ni 25 at.% (figure S2). For the unsupported nanoparticles, however, no significant difference between the composition close to the edge and the overall composition was found.

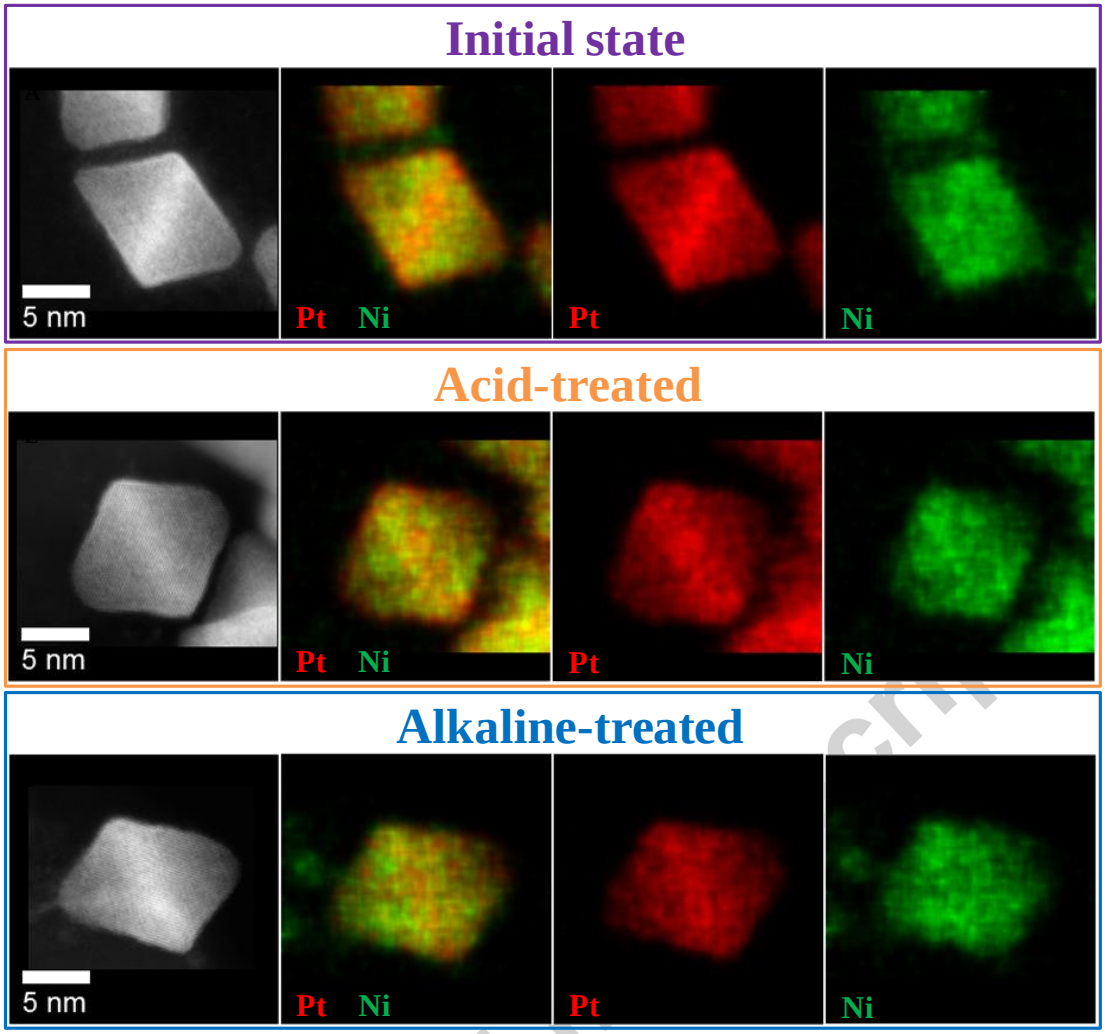

Fig 2. HAADF-STEM images and EDX composition maps of PtNi octahedral nanoparticles. High resolution HAADF-STEM images of the nanoparticles oriented close to ⟨110⟩ in the initial state (A), after acid treatment (E) and after alkaline treatment (I). EDX composition maps (B, F, J), showing Pt (red, C, G, K) and Ni (green, D, H, L) distributions, of the corresponding octahedral nanoparticles, respectively.

The nanoparticles show a similar morphology before and after alkaline treatment. The existence of hydroxide anions in the washing medium in combination with the high oxophility of Ni makes it likely that Ni-hydroxides are forming near the catalyst surface. According to the Pourbaix diagram, these cannot chemically dissolve under strong alkaline conditions. A Pt-rich stripe located at the center of the nanoparticles is still visible, while Ni enrichment at the facets and between adjacent nanoparticles has intensified (figures 2 I-L). The formation of a

pronounced Pt-skin is not observed. Only the corners seem to be slightly more rounded in most cases compared to the original octahedra. The circle diameter in figure S1C is 3.8 nm. This indicates the migration of the Pt surface atoms already starts under this treatment. The acid processing dissolves surface Ni, leaving low coordinated Pt atoms along the nanoparticles surface, which are more likely to be detached and thus leading to more rounded corners. The average composition of the corresponding alkaline treated octahedra is Pt 62 at.% and Ni 38 at.%. Taking into account the error in measurement of the EDX quantification (± 2 at. %), we can conclude that the different surface treatments do not cause notable changes in the overall nanoparticle composition. However, the EDX maps do point to differences in the distribution of the elements on the surface of the nanoparticles. The acid-treated sample demonstrates a Pt-skin, while Ni is more present at the outer part of the facets of the alkaline-treated nanoparticles.

The atomic composition was also determined by ICP-MS, as well as the Pt loading of the PtNi/C catalysts. The sample washed with acetic acid showed a Pt 60 at.% and Ni 40 at.% atomic composition with a Pt loading of 18.6 % wt. On the other hand, when the as-prepared supported nanoparticles are cleaned under alkaline conditions, an electrocatalyst with atomic composition of Pt 57 at.% and Ni 43 at.% and 14.7 % wt. of Pt loading is produced. The little differences may be due to experimental errors of the ICP-MS quantification. Interestingly, both EDX and ICP-MS measurements show slightly higher Ni concentration in the base-treated sample. Thus, we resolve that the octahedral PtNi nanoparticles have a ~$Pt_{1.5}Ni$ bulk composition, independently of the washing protocol applied, but we also presume that the slightly lower Ni content of the acid-treated sample might be caused by the superficial leaching of the non-noble metal during the decontamination procedure. In addition, the differences between the Pt loadings on the carbon in both samples are also a consequence of the different cleaning protocols. It can be concluded that the washing method using alkali leads to a partial loss of the nanoparticles, which is understandable as the process contains more manipulation steps.

To further examine the surface characteristics of the PtNi octahedra, XPS was employed to both determine the chemical composition and the oxidation states of the components present at the outer atomic layers of the nanoparticles. XPS spectra from the Pt-4f (A, C) and Ni-2p (B, D) core level regions of the acid and alkaline-treated PtNi octahedra are shown in figure 3. The surface Pt/Ni atomic ratios were 4.4 ($Pt_{81}Ni_{19}$) and 1.6 ($Pt_{62}Ni_{38}$), respectively, which were estimated by integrating the peak area in the XPS spectra after the background correction. This quantification confirmed that the surfaces of both bimetallic samples are clearly different. The washing procedure using alkaline conditions basically preserves the bulk composition of the nanoparticles, while a Pt-rich skeleton-structure surface is shown for the sample chemically leached under acidic conditions. Table 1 reports the binding energies (BE) from the deconvolution of the XPS spectra. The Pt-4f spectra were fitted with two doublets ($4f_{7/2}$ and $4f_{5/2}$) corresponding to Pt^0 and Pt^{2+} (assigned to species like PtO and $Pt(OH)_2$), which are in agreement with those reported elsewhere [41, 42]. The results do not reveal significant differences between the oxidation states of Pt in both specimens. By comparing the relative intensities of the peaks due to Pt^0 and those of PtO and $Pt(OH)_2$ it is possible to say that Pt is predominately metallic at the surface of both PtNi samples. In addition, by the slight differences between the BE of the Pt^{2+} species as consequence of the different decontamination treatments, we suggest that PtO is the species formed on the acid-treated sample, while $Pt(OH)_2$ is more present at the alkaline-treated specimen. The structure of the Ni-2p core-level spectra is more complicated due to the presence of satellite peaks (861 and 863 eV) nearby the main peaks, which are attributed to multi-electron excitation. Two doublets ($2p_{3/2}$ and $2p_{1/2}$) were found. Taking the satellite peak into account, the $Ni2p_{3/2}$ peak could be deconvoluted into three peaks assigned to three different oxidation states: Ni^0, Ni^{2+} and Ni^{3+}. This means that, besides the metallic Ni, this element is mainly present in the form of NiO, $Ni(OH)_2$, Ni_2O_3 and/or NiOOH at the surfaces[43-46]. The comparison between the relative intensity of the peaks points out that the remaining non-noble metal at the surface of the nanoparticles after acidic chemical leaching is mostly present as metallic Ni, while O-containing species are chiefly formed when PtNi are decontaminated in alkaline media. Thus, the XPS results revealed that the acidic-treated PtNi

nanooctahedra present a Pt-rich surface mainly composed of Pt^0 and Ni^0, while the sample treated under alkaline conditions mostly preserves the bulk composition and contains Pt^0, NiO and $Ni(OH)_2$ species at the surface. Note that the XPS data for the alkaline-treated sample may also include the signal from compounds containing Ni between the nanoparticles.

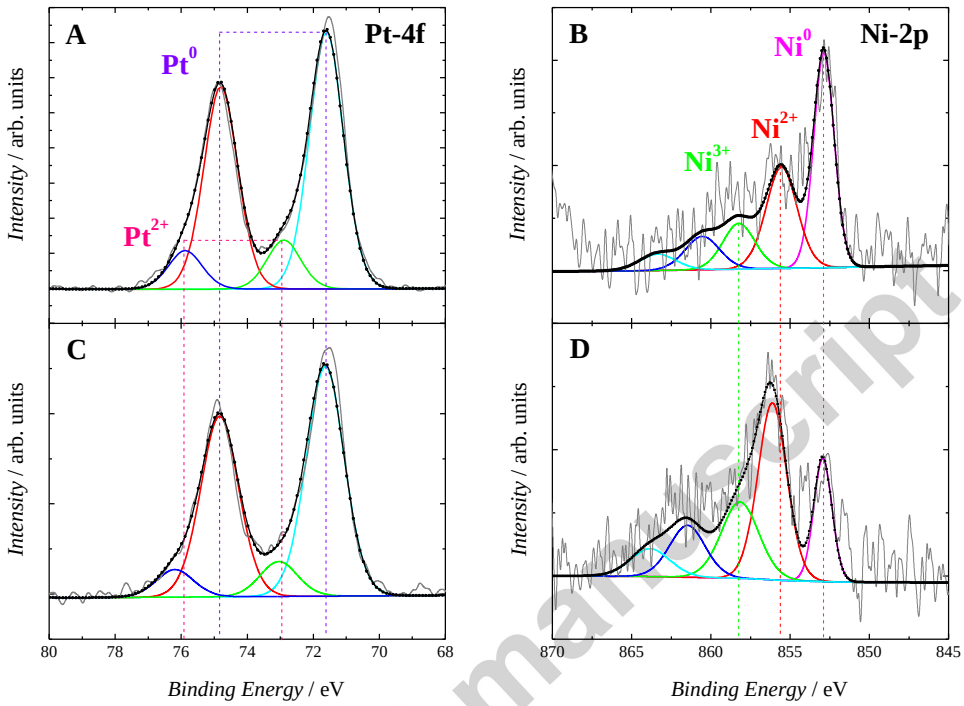

Fig 3. XPS spectra from Pt-4f and Ni-2p core level regions of PtNi octahedral nanoparticles supported on carbon acquired at room temperature. Acidic-treated (A,B) and alkaline-treated (C,D) PtNi octahedra.

Table 1. XPS data and the possible chemical states for Pt and Ni.

Sample	XPS of Pt4f (BE in eV)	XPS of Ni2p (BE in eV)
Acid-treated	71.6 (Pt^0), 72.9 (PtO), 74.8 (Pt^0), 75.8 (PtO)	852.8 (Ni^0), 855.6 (NiO), 858.2(Ni_2O_3), 860.5 and 863.4 (satellites)
Alkaline-treated	71.6 (Pt^0), 73.1 ($Pt(OH)_2$), 74.8 (Pt^0), 75.8 ($Pt(OH)_2$)	852.9 (Ni^0), 856.1 ($Ni(OH)_2$), 858.2 (NiOOH), 861.5 and 863.8 (satellites)

3.2. Electrochemical Characterization

Subsequently, the voltammetric characterization of the PtNi/C electrocatalysts was performed. For the sake of comparison, the electrochemical profiles and catalytic activity of the bimetallic catalysts are contrasted with the electrochemical response of (100)-(111) preferentially oriented Pt nanoparticles synthesized by the method described by Kang et al. [32] and decontaminated under alkaline conditions [36]. Figure S3 shows some representative TEM images of the unsupported and carbon supported (24.4 % wt, determined by thermogravimetry analysis) Pt nanoparticles with average size of 10.4 ± 1.2 nm. It is important to point out that the decontamination protocol under alkaline conditions has been shown to be effective also for carbon supported nanoparticles, as demonstrated in figure S4. The good definition and the symmetry of the adsorption states in all samples are indicative of the adequate surface cleanliness. The results are in agreement with those previously obtained for nanoparticles with cubic truncated shape (NP_{trunc}) [36, 47].

Figures 4A and 4C show the electrochemical characterization of both samples of PtNi nanooctahedra (acid and alkaline treated) by using the thin-film-rotating disk electrode (TF-RDE) technique in the three most frequently used aqueous supporting electrolytes: 0.5 M H_2SO_4, 0.1 M $HClO_4$ and 0.1 M NaOH. Cyclic voltammograms (CVs) were recorded in the potential range of 0.05-0.9 V (vs. reversible hydrogen electrode (RHE)) in order to avoid surface oxidation and trying to preserve the superficial structure before ORR measurements. The analysis of the characteristic voltammetric features shows that the electrochemical responses of both PtNi samples are very similar. H_{upd} peaks appear at E<0.35 V in the CVs recorded in acidic media, the features are better defined in sulfuric acid due to the specific adsorption of the sulfate anions. In alkaline media, these H_{upd} peaks shift toward higher potential values, being the OH adsorption also involved in the features at E<0.5 V [48, 49]. It is worth noting the presence of signals between 0.5-0.65 V in sulfuric acid media, which resembles the sulfate adsorption/desorption on bidimensionally ordered (111) terraces in Pt surfaces [47]. In

perchloric and alkaline media, a featureless flat signal between 0.5-0.75 V is followed by the characteristic OH adsorption contribution in the potential range between 0.75-0.9 V. This adsorption is inhibited in sulfuric acid due to the stronger adsorption of sulfate anions. The voltammetric profiles of both octahedral PtNi samples are compared to each other and related to (100)-(111) preferentially oriented Pt nanoparticles in figure S5. Interestingly, H_{upd} formation in both sulfuric and perchloric acid occurs in a narrower potential range (from 0.05 to 0.35 V) than on pure Pt nanoparticles, on which it extends up to 0.45 V. On the other hand, in alkaline medium it is possible to observe a positive shift in OH adsorption. These changes for the onset of Pt-OH_{ad} formation, related to Pt nanoparticles, points out the weaker chemisorptions of oxygenated species on PtNi surfaces, which is the key point for enhancing the ORR kinetics [50, 51]. This fact was previously observed for Pt_3Ni single crystal electrodes with basal orientations in perchloric acid solution [10].

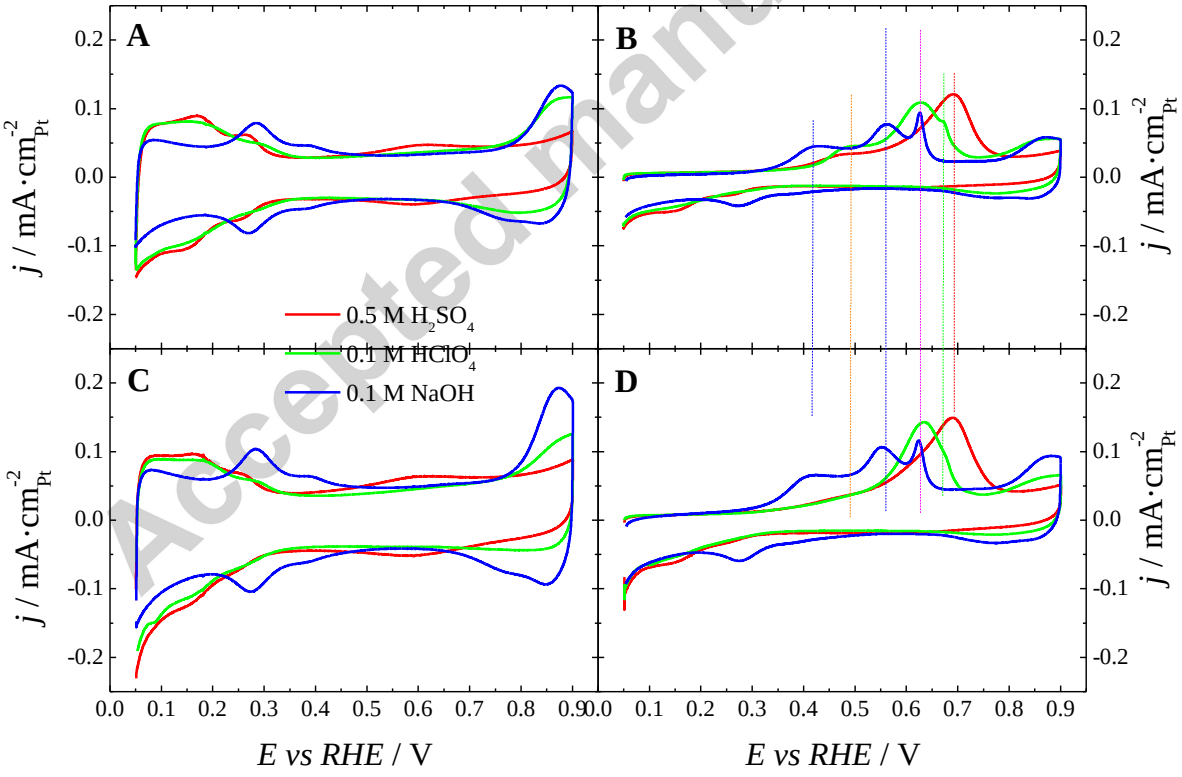

Fig 4. Voltammetric (50 $mV \cdot s^{-1}$) and CO stripping (20 $mV \cdot s^{-1}$) profiles of carbon supported PtNi octahedral nanoparticles after acidic (A, B) and alkaline (C, D) treatment in different supporting electrolytes: 0.5 M H_2SO_4 (red), 0.1 M $HClO_4$ (green) and 0.1 M NaOH (blue).

The specific surface areas (SSAs) calculated from the charge involved in the H_{upd} region of the voltammograms recorded in sulfuric acid, after double layer subtraction, were 13.28, 10.33 and 9.56 $m^2 \cdot g_{Pt}^{-1}$ for the Pt NP_{trunc}, acid-treated and alkaline-treated PtNi nanoparticles, respectively. These results are included in Table 2. As expected, pure Pt nanoparticles present higher SSA, since they are slightly smaller than the bimetallic samples. The differences between the two PtNi samples are likely caused by the removal of superficial Ni during the acidic treatment, which expose more surface Pt atoms (where the H_{upd} takes place) with low coordination. We have used electrochemical surface area obtained by the H_{upd} to calculate the specific activity, since it was demonstrated to be independent of the voltammetric history and little affected by previous CO stripping steps [52]. However, we are aware that the values obtained by this method are smaller in magnitude than those obtained by CO-ECSA, which can lead to an overestimation of the true specific ORR activity.

Figures 4B and 4D show the oxidation of the CO layer on the surface of the PtNi nanoparticles in the three different supporting electrolytes. The CO was adsorbed at 0.1 V until complete blockage of the surface, which was monitored by cycling the electrode between 0.05 and 0.35 V. After elimination of dissolved CO by bubbling Ar, the adsorbed CO was subsequently oxidized in a single sweep. It is possible to clearly observe the effect of pH and adsorbed anions on the peak potential and sharpness of the CO stripping profile. As with Pt surfaces, the onset for the CO oxidation follows the trend NaOH < $HClO_4$ < H_2SO_4 [53]. The different mobility of the CO molecules on the surfaces, determined by the interfacial pH and the presence of adsorbed species, is responsible for the different CO oxidation responses in acidic or alkaline media [54, 55]. The higher oxidation peak potential for sulfuric acid is due to the specific adsorption of sulfate anions, which hinders the adsorption of the O-containing species necessary for CO oxidation. The multiple peaks appearing in the CO stripping voltammetry correspond to the oxidation on different surface sites. There is a notable pre-wave of the oxidation profile in 0.1 M NaOH at 0.42 V, and two differentiated oxidation peaks at 0.56 and 0.69 V. This pre-

wave feature has been related to CO oxidation on sites which have Ni or Ni-hydroxides nearby [56], assuming that the Ni species (very oxophilic) serve as supply of active oxygenates to oxidize CO. It should be noted that the intensity of this signal is higher for the alkaline-treated sample, where the amount of surface Ni is greater. Although the CO oxidation profiles for both samples are rather similar in all media, some differences can be observed between the CVs recorded in perchloric and sulfuric acid: i) the acid-treated sample presents a pre-wave at 0.49 V (more noticeable in perchloric acid) that is not observable for the alkaline-treated nanoparticles, ii) the CO stripping in 0.1 M $HClO_4$ shows a shoulder at 0.67 V, which is better defined for the acid-treated sample than for the alkaline-treated one, and iii) the OH adsorption is more pronounced in the acid-treated nanoparticles, as shown by the charge involved above 0.8 V in the CVs recorded in perchloric acid. Taking into account that the washing procedure using acetic acid caused a chemical leaching of the superficial Ni atoms leading to a Pt skeleton-type structure, the presence of the pre-wave and the multiplicity in the oxidation peaks can be justified by the presence of low coordinated surface Pt atoms, in comparison with the catalyst washed under alkaline conditions that keeps the superficial Ni atoms.

3.3. Oxygen Reduction on octahedral PtNi/C and (100)-(111)-Pt/C Catalysts

The electrocatalytic activity towards ORR of both octahedral PtNi/C samples was evaluated in 0.1 M $HClO_4$ and 0.1 M NaOH solutions, and compared with the results obtained for Pt (100)-(111) preferentially oriented (faceted) nanoparticles. Different electrochemical pretreatments were applied before ORR polarization curves were obtained, namely testing the activity directly in perchloric acid, or after applying a previous step in sulfuric acid. In addition, the electrocatalytic activity was tested after electrochemical dealloying of the surface of the bimetallic nanoparticles (50 cycles in 0.5 M H_2SO_4 solution between 0.05 and 0.9 V at a sweep rate of 50 $mV \cdot s^{-1}$), and after applying excursions up to high potentials (1.4 V) which causes a strong surface disordering of the three samples. Figure S6 shows the polarization curves of the

three samples studied in an O_2-saturated 0.1 M $HClO_4$ solution, when the catalysts' activities are measured directly in this medium, or after applying a previous step in sulfuric acid consisting in two processes of CO adsorption and electrochemical oxidation. This procedure results in much cleaner particles, since CO molecules are capable of displacing the remaining impurities occasionally present at the surface of the nanoparticles [57]. The pretreatment does not have a significant effect on the acid-treated PtNi and pure Pt nanoparticles, however, it does improve the activity of the alkaline-treated PtNi. This can be seen by the positive shift of the half-wave potential, $E_{1/2}$, commonly used to evaluate the electrocatalytic activity of a catalyst. It is important to mention that the polarization curves in our study are not iR-corrected.

CO stripping experiments were also performed in perchloric acid for this latter sample, which results in similar catalytic activity as when this procedure is carried out in sulfuric acid. Once discarded the effect of the nature of the supporting electrolyte, CO adsorption and following electrooxidation may be the responsible of this activity enhancement. Some studies have reported on the healing of the surface defects as a consequence of electrochemical CO annealing [58, 59], or atomic segregation phenomena induced by CO environment [60]. Nevertheless, a more plausible explanation for the increase in catalytic activity towards ORR is the partial dissolution of nickel and the high level of cleanliness of the surface.

It was reported that OH coming from the hydroxide layer can react with the CO adsorbed on the Pt atoms [45, 61]:

$$Ni\text{-}OH_{ad} + Pt\text{-}CO_{ad} \rightarrow CO_2 + Pt + Ni + H^+ + e^- \qquad (1)$$

In this way, the excessive Ni loading that lowers the catalytic activity by hindering the available Pt [34, 39] would be partially dissolved in acidic media after applying two steps of CO stripping.

Based on these results, the following experiments of ORR were carried out after this previous step in sulfuric acid. Figure S7 shows the classic set of current-potential curves for ORR in

0.1 M $HClO_4$ measured at different rotation rates and the Koutecky-Levich (K-L) plots for the three samples. The K-L equation (2) was used to analyze the RDE data on O_2 reduction:

$$\frac{1}{j} = \frac{1}{j_k} + \frac{1}{j_d} = -\frac{1}{nFkC_{O_2}^b} - \frac{1}{0.62nFD_{O_2}^{2/3}\nu^{-1/6}C_{O_2}^b\omega^{1/2}} \qquad (2)$$

where j is the measured current density, j_k and j_d are the kinetic and diffusion-limited current densities, respectively, n is the number of electrons transferred per O_2 molecule, k is the rate constant for O_2 reduction, F is Faraday's constant (96485 C mol^{-1}), ω is angular frequency of rotation, $\omega=2\pi f/60$, f is the RDE rotation rate in r.p.m, $C_{O_2}^b$ is the concentration of O_2 in the bulk ($1.26\cdot10^{-3}$ mol dm^{-3}), D_{O_2} is the diffusion coefficient of O_2 ($1.93\cdot10^{-5}$ cm^2 s^{-1}) and ν is the kinematic viscosity of the electrolyte ($1.01\cdot10^{-2}$ cm^2 s^{-1}). The number of electrons transferred (n) was calculated from the slopes of the K-L plots at 0.3-0.6 V. The value of n was calculated to be ~ 4 in this potential window for both samples of PtNi octahedra and the pure Pt sample, pointing out the complete reduction of O_2 to H_2O on the surface of these nanoparticles.

Figure 5 shows a comparison of the O_2 reduction polarization curves of the catalysts studied, both in acidic and alkaline media. In perchloric acid (figure 5A), the $E_{1/2}$ values increase in the sequence: (100)-(111)-Pt < alkaline treated-PtNi ≈ acid treated-PtNi. In alkaline medium, the bimetallic nanocatalyst washed under acidic conditions displays better electrocatalytic activity, following the trend: (100)-(111)-Pt < alkaline treated-PtNi < acid treated-PtNi. From these curves, the characteristic kinetic current at 0.9 V was obtained for each electrocatalyst using the K-L equation (figure S7D). These values were normalized to the H_{upd}-ECSA and to the Pt mass to calculate the specific and the mass activity, respectively (Table 2). Both PtNi/C electrocatalysts were more active than our shaped Pt/C and commercial Pt/C [62] towards ORR in both acidic and alkaline media. The mass activities at 0.9 V in perchloric acid are in agreement with those reported for nanoparticles with similar edge lengths [34]. However, the specific activities here reported are higher, most likely due a cleaner state of the surface of the nanoparticles.

In comparison with acidic media, studies carried out in alkaline media are scarce [63, 64]. Our results show that the specific and mass activities at 0.9 V are lower in alkaline than in acidic media (Table 2). Similar behavior was observed for Pt single crystal electrodes [26]. Interestingly, both samples of PtNi octahedra display comparable catalytic activity in acidic medium, while the acid-treated PtNi is more active under alkaline conditions. The ORR kinetics on a Pt surface depends on the strongly adsorbed oxygen-containing species [7], and it has been previously reported that an increase in the Ni surface concentration leads to an increase in the binding energy of O_2 [65]. We also suggest that the higher Ni content on the surface of the alkaline-treated PtNi nanoparticles would produce a hydroxide layer thus hindering the O_2 reduction. It is worth mentioning that the O_2 polarization curve of the (100)-(111)-Pt nanoparticles in alkaline media resembles the behavior of Pt stepped surfaces [25], showing again the faceted character of this sample and the high level of cleanliness.

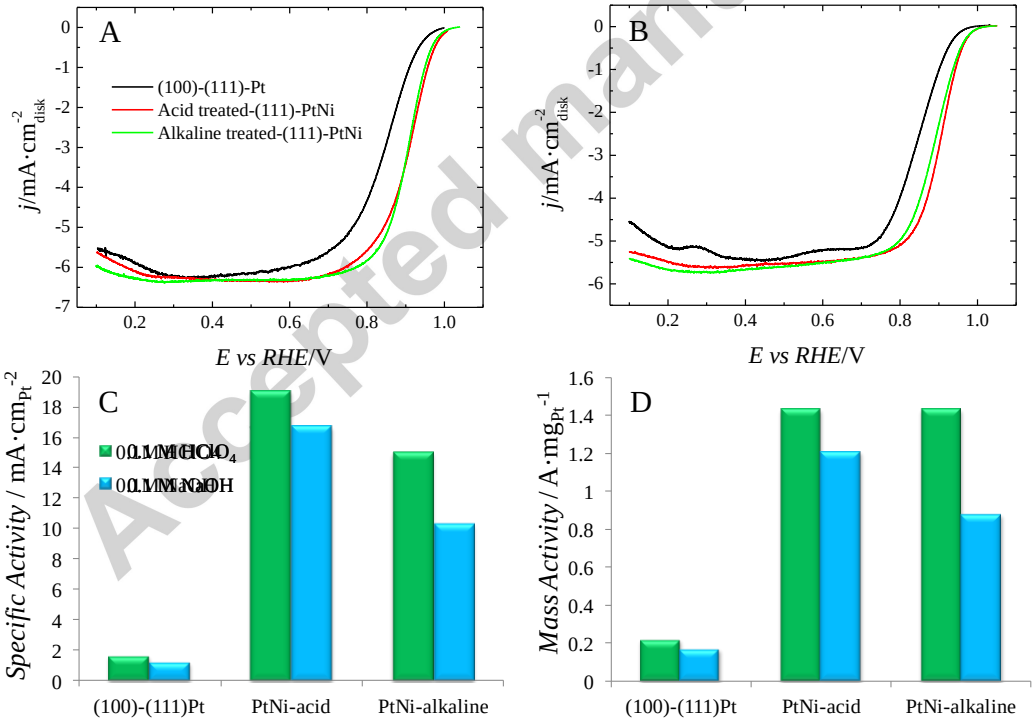

Fig 5. ORR polarization curves of the octahedral Pt-Ni/C electrocatalysts, acid-treated (red line) and alkaline-treated (green line), and (100)-(111) preferentially oriented Pt (black line) nanoparticles in O_2-saturated 0.1 M $HClO_4$ (A) and 0.1 M NaOH (B) solutions. Scan rate, 10 mV/s. Rotation speed,

1600 rpm. The currents were normalized to the geometric area of the rotating disk electrode (0.0707 cm^2). Comparison of specific (C) and mass (D) activities in 0.1 M $HClO_4$ (green bars) and 0.1 M NaOH (blue bars) at 0.9 V.

Table 2. Electrocatalytic properties of Pt-Ni octahedral nanoparticles with different surface composition, and (100)-(111)-Pt nanoparticles

Catalyst	Pt:Ni ratio		SSA_{Pt} ($m^2 \cdot g_{Pt}^{-1}$)	SA* ($mA \cdot cm^{-2}$)		MA* ($A \cdot mg_{Pt}^{-1}$)	
	Surface (XPS)	Bulk (ICP)		0.1 M $HClO_4$	0.1 M NaOH	0.1 M $HClO_4$	0.1 M NaOH
Acid-treated	4.39	1.53	7.53	19.02	16.71	1.38	1.16
Alkaline-treated	1.62	1.31	9.56	14.97	10.31	1.39	0.86
(100)-(111)-Pt	-	-	13.28	1.66	1.23	0.22	0.17

* Specific (SA) and mass (MA) activities were evaluated at 0.9 V.

Previous studies on PtNi catalysts revealed that dealloying under electrochemical conditions in a process called "electrochemical activation" results in Pt-rich nanoparticles with a skeleton structure that exhibits higher ORR activity by leaching the Ni present at the {111} facets [39]. Based on these results, after testing the ORR activities reported before, we applied 50 cycles in a 0.5 M H_2SO_4 solution between 0.05-0.9 V at a sweep rate of 50 $mV \cdot s^{-1}$ and the bimetallic electrocatalysts were evaluated again towards ORR (figure S8). Although traditional electrochemical activation involves cycling up to higher potentials, we set the upper potential of 0.9 V to reasonably protect the surface structure of the nanoparticles [66]. As can be seen, the dealloying process causes an improvement in the electrocatalytic activity of both PtNi samples. This cycling pretreatment in acid environments is known to selectively leach the surface Ni hydroxide species, leaving low coordinated Pt atoms that could serve as active adsorption sites for water activation [56, 64, 67, 68]. In this sense, the catalytic activity enhancement is more remarkable for the alkaline-treated PtNi/C sample (Table S1), where the gradually

electrochemical Ni dissolution seems to favor the kinetics of the ORR in comparison to the more aggressive acid chemical leaching.

3.4. Effect of Surface Disordering on the Electrocatalytic Activity

The effect of electrochemical activation on shape-controlled Pt nanoparticles has been recently reported, showing that only 25 potential cycles are sufficient to induce a complete surface disordering and significant catalyst degradation [66]. Figure S9 shows representative HAADF-STEM images of the acid and alkaline-treated octahedra after applying 50 potential cycles up to 1.4 V in sulfuric medium at a sweep rate of 50 $mV \cdot s^{-1}$. High resolution HAADF-STEM images and EDX elemental mapping of both samples are displayed in figure 6. In both cases the HAADF-STEM images show markedly concave octahedra. The EDX maps for Pt and Ni indicate a loss of Ni at the facets compared to the acid-treated octahedra. However, EDX quantification yields a whole particle composition of Pt 72 at.% and Ni 28 at.% for 50 cycles-acid-treated and Pt 70 at.% and Ni 30 at.% for the 50 cycles-base-treated octahedra. Thus, after this rough treatment both samples evolve to a similar strong concave shape with a round bright stripe at the outer part. This is chiefly due to Ni and Pt dissolution at the facets of the initial octahedra.

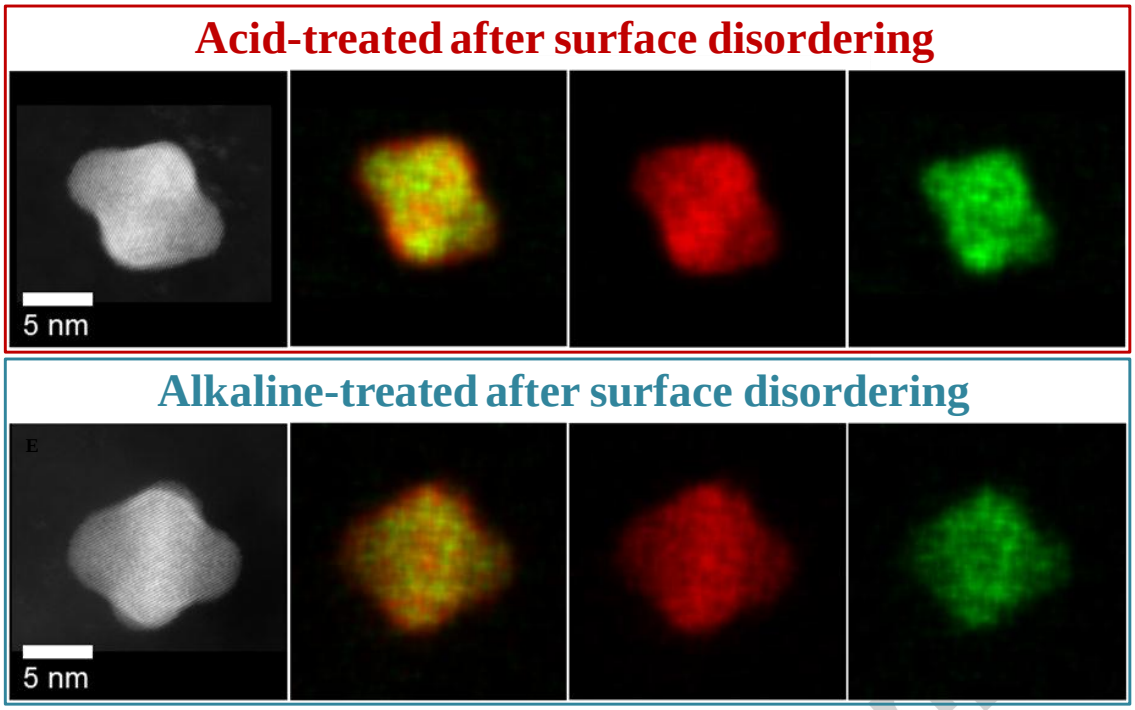

Fig 6. HAADF-STEM images and EDX composition maps of PtNi octahedral nanoparticles after electrochemical surface disordering: acid-treated sample (A-D) and alkaline-treated sample (E-H).

The effect of surface disordering after electrochemical cycling on the electrocatalytic activity has been tested for ORR and CO electrooxidation, which are both structure sensitive reactions. Figure S8 shows the polarization curves in 0.1 M $HClO_4$ solution before and after applying 50 potential cycles of electrochemical activation [66]. All catalysts experience a decay on their electrocatalytic activity (Table S1), mainly due to the loss of the well-ordered structure of the {111} facets and also {100} facets in the case of pure Pt nanoparticles. From the O_2 reduction curves in figure S8 it seems that the loss in activity of this later catalyst is less accused. Taking into account that the (100) surface is the less active for ORR in both acid and alkaline media, and that the Pt NP_{trunc} are mainly composed by {100} facets, a small drop in activity is expected when these faceted catalysts evolve into polyoriented nanoparticles.

Previous studies on CO electrooxidation using Pt single electrodes and shaped nanoparticles demonstrated the surface structure sensitiveness of this process [36, 69, 70]. In this regard, this

reaction can be used as a probe to detect surface structure changes, for example, after electrochemical activation. Besides the electrocatalytic activity towards ORR, the changes induced in the voltammetric profiles and CO stripping in 0.5 M H_2SO_4 and 0.1 M NaOH solutions after electrochemical activation were also studied. As can be seen in figures S10 and S11, both the blank voltammetry and CO oxidation peak suffer several changes. The most noticeable effect is the increasing of the charge in the H_{upd} region, mainly due to further dissolution of the superficial nickel and an increase in surface roughness due to the evolution of the characteristic faceted structure of the nanoparticles (bidimensional domains) into steps and kinks sites. Moreover, in sulfuric acid, it is possible to observe an increase in the current intensity of the peak at 0.26 V and the disappearance of the signal at 0.6 V. The CO stripping profile in this medium evolves into the typical response of Pt polyoriented nanoparticles [36]. These changes are not so pronounced in alkaline medium, where the voltammetric profiles of the blank and the CO stripping remain basically the same, being the shift of the oxidation peaks towards more positive potentials the most relevant swap. As it has been previously mentioned, the dissolution of the superficial nickel could be the responsible of the changes in catalytic activity. In the case of CO oxidation, nickel dissolution would decrease the activity (equation 1) [45, 61]. Nevertheless, excessive Ni loading would lower the catalytic activity by hindering the available Pt. This effect would be overcome by the electrochemical leaching and surface disordering caused by potential cycling. In this regard, it can be observed a slight negative shift of the potential where the adsorption of OH species takes place, which would decrease the catalytic activity for ORR, as stated and demonstrated previously. Similar effects were obtained for the alkaline-treated sample, as shown in figure S11. These results manifest the outmost importance not only of the pH of the pretreatment environment of the electrocatalysts, but also the special care that must be exercised in the choice of potential limits when studying multimetallic shaped nanoparticles.

4. Conclusions

In this study, the effect of interfacial pH during the surface decontamination of octahedral PtNi/C electrocatalysts has been analyzed. The particles were treated in strong acid or alkaline conditions, and the impact on their surface elemental distribution and composition, and the influence on their electrochemical response and catalytic activity have been explored. The use of alkaline conditions has proved to be useful for cleaning alloyed nanoparticles while preserving their bulk composition on the surface. In comparison, the method based on acid chemical leaching that abruptly removes the non-noble metals from the structure. Ex situ characterization techniques, such as STEM, EDX elemental mapping and XPS have revealed significant compositional changes in solid alloy surfaces at the nanoscale level, induced by the chemical environment where the electrocatalysts are produced. In the same way, in situ electrochemical measurements like cyclic voltammetry and CO oxidation on a given supporting electrolyte have shown that the modifications prompted under operation conditions are the key to understand the catalyst reactivity. Both kinds of electrocatalysts have been proved to be very active either in acidic or basic media towards ORR, showing better catalytic properties than shaped Pt nanoparticles and exhibiting an improvement factor of 10 versus commercial Pt (mass activity @ 0.9 V). Strong compositional and morphological changes have been demonstrated when subjecting these materials to electrochemical activation, producing a decay in the catalytic activity and emphasizing the special care needed when handling shaped nanoparticles. In conclusion, a combination of ex situ and in situ techniques have clearly demonstrated the importance of the interfacial pH of the pretreatment environment on the catalytic behavior of alloy electrocatalysts. We believe that our findings will aid the development of strategies for selectively controlling the surface composition and the presence of distinct active species, thus tuning their catalytic performance.

Acknowledgments

This work was carried out under financial support of MICINN (project no. CTQ2013-44083-P). M.H. and M.G. thank the Deutsche Forschungsgemeinschaft (DFG) for financial support within the grant HE7192/1-1, and to Katherine MacArthur for helpful discussions. P.S. acknowledges partial financial support by the German Research Foundation (DFG) through grants STR 596/5-1 and STR 596/4-1.

References

[1] J. Tollefson, Nature 464 (2010) 1262-1264.

[2] M.K. Debe, Nature 486 (2012) 43-51.

[3] N.M. Marković, T.J. Schmidt, V. Stamenković, P.N. Ross, Fuel Cells 1 (2001) 105-116.

[4] J.K. Nørskov, J. Rossmeisl, A. Logadottir, L. Lindqvist, J.R. Kitchin, T. Bligaard, H. Jónsson, J. Phys. Chem. B 108 (2004) 17886-17892.

[5] P. Strasser, S. Koh, T. Anniyev, J. Greeley, K. More, C. Yu, Z. Liu, S. Kaya, D. Nordlund, H. Ogasawara, M.F. Toney, A. Nilsson, Nature Chem. 2 (2010) 454-460.

[6] S. Prabhudev, M. Bugnet, C. Bock, G.A. Botton, ACS Nano 7 (2013) 6103-6110.

[7] V. Stamenkovic, B.S. Mun, K.J.J. Mayrhofer, P.N. Ross, N.M. Markovic, J. Rossmeisl, J. Greeley, J.K. Norskov, Angew. Chem. Int. Ed. 45 (2006) 2897-2901.

[8] I.E.L. Stephens, A.S. Bondarenko, F.J. Perez-Alonso, F. Calle-Vallejo, L. Bech, T.P. Johansson, A.K. Jepsen, R. Frydendal, B.P. Knudsen, J. Rossmeisl, I. Chorkendorff, J. Am. Chem. Soc. 133 (2011) 5485-5491.

[9] V.R. Stamenkovic, B.S. Mun, M. Arenz, K.J.J. Mayrhofer, C.A. Lucas, G. Wang, P.N. Ross, N.M. Markovic, Nat. Mater. 6 (2007) 241-247.

[10] V.R. Stamenkovic, B. Fowler, B.S. Mun, G.F. Wang, P.N. Ross, C.A. Lucas, N.M. Markovic, Science 315 (2007) 493-497.

[11] G.A. Attard, J.-Y. Ye, A. Brew, D. Morgan, P. Bergstrom-Mann, S.-G. Sun, J. Electroanal. Chem. 716 (2014) 106-111.

[12] V.R. Stamenkovic, B.S. Mun, K.J.J. Mayrhofer, P.N. Ross, N.M. Markovic, J. Am. Chem. Soc. 128 (2006) 8813-8819.

[13] J. Greeley, I.E.L. Stephens, A.S. Bondarenko, T.P. Johansson, H.A. Hansen, T.F. Jaramillo, J. Rossmeisl, I. Chorkendorff, J.K. Nørskov, Nature Chem. 1 (2009) 552-556.

[14] P. Malacrida, M. Escudero-Escribano, A. Verdaguer-Casadevall, I.E.L. Stephens, I. Chorkendorff, J. Mater. Chem. A 2 (2014) 4234-4243.

[15] P. Hernandez-Fernandez, F. Masini, D.N. McCarthy, C.E. Strebel, D. Friebel, D. Deiana, P. Malacrida, A. Nierhoff, A. Bodin, A.M. Wise, J.H. Nielsen, T.W. Hansen, A. Nilsson, I.E.L. Stephens, I. Chorkendorff, Nature Chem. 6 (2014) 732-738.

[16] T.P. Johansson, E.T. Ulrikkeholm, P. Hernandez-Fernandez, M. Escudero-Escribano, P. Malacrida, I.E.L. Stephens, I. Chorkendorff, Phys. Chem. Chem. Phys. 16 (2014) 13718-13725.

[17] T.P. Johansson, E.T. Ulrikkeholm, P. Hernandez-Fernandez, P. Malacrida, H.A. Hansen, A.S. Bandarenka, J.K. Nørskov, J. Rossmeisl, I.E.L. Stephens, I. Chorkendorff, Top. Catal. 57 (2014) 245-254.

[18] T. Toda, H. Igarashi, H. Uchida, M. Watanabe, J. Electrochem. Soc. 146 (1999) 3750-3756.

[19] C. Wang, N.M. Markovic, V.R. Stamenkovic, ACS Catal. 2 (2012) 891-898.

[20] D. Wang, Y. Yu, H.L. Xin, R. Hovden, P. Ercius, J.A. Mundy, H. Chen, J.H. Richard, D.A. Muller, F.J. DiSalvo, H.D. Abruña, Nano Lett. 12 (2012) 5230-5238.

[21] M. Shao, A. Peles, K. Shoemaker, Nano Lett. 11 (2011) 3714-3719.

[22] R. Loukrakpam, J. Luo, T. He, Y. Chen, Z. Xu, P.N. Njoki, B.N. Wanjala, B. Fang, D. Mott, J. Yin, J. Klar, B. Powell, C.-J. Zhong, J. Phys. Chem. C 115 (2011) 1682-1694.

[23] R.M. Arán-Ais, F. Dionigi, T. Merzdorf, M. Gocyla, M. Heggen, R.E. Dunin-Borkowski, M. Gliech, J. Solla-Gullón, E. Herrero, J.M. Feliu, P. Strasser, Nano Lett. 15 (2015) 7473-7480.

[24] F.J. Perez-Alonso, D.N. McCarthy, A. Nierhoff, P. Hernandez-Fernandez, C. Strebel, I.E.L. Stephens, J.H. Nielsen, I. Chorkendorff, Angew. Chem. Int. Ed. 51 (2012) 4641-4643.

[25] R. Rizo, E. Herrero, J.M. Feliu, Phys. Chem. Chem. Phys. 15 (2013) 15416-15425.

[26] A.M. Gomez-Marin, R. Rizo, J.M. Feliu, Catal. Sci. Technol. 4 (2014) 1685-1698.

[27] N.M. Marković, R.R. Adžić, B.D. Cahan, E.B. Yeager, J. Electroanal. Chem. 377 (1994) 249-259.

[28] H.A. Gasteiger, N.M. Markovic, Science 324 (2009) 48-49.

[29] S.I. Choi, S. Xie, M. Shao, J.H. Odell, N. Lu, H.C. Peng, L. Protsailo, S. Guerrero, J. Park, X. Xia, J. Wang, M.J. Kim, Y. Xia, Nano Lett. 13 (2013) 3420-3425.

[30] C. Chen, Y. Kang, Z. Huo, Z. Zhu, W. Huang, H.L. Xin, J.D. Snyder, D. Li, J.A. Herron, M. Mavrikakis, M. Chi, K.L. More, Y. Li, N.M. Markovic, G.A. Somorjai, P. Yang, V.R. Stamenkovic, Science 343 (2014) 1339-1343.

[31] J. Zhang, J. Fang, J. Am. Chem. Soc. 131 (2009) 18543-18547.

[32] Y. Kang, J.B. Pyo, X. Ye, R.E. Diaz, T.R. Gordon, E.A. Stach, C.B. Murray, ACS Nano 7 (2013) 645-653.

[33] Y. Kang, M. Li, Y. Cai, M. Cargnello, R.E. Diaz, T.R. Gordon, N.L. Wieder, R.R. Adzic, R.J. Gorte, E.A. Stach, C.B. Murray, J. Am. Chem. Soc. 135 (2013) 2741-2747.

[34] S.-I. Choi, S. Xie, M. Shao, N. Lu, S. Guerrero, J.H. Odell, J. Park, J. Wang, M.J. Kim, Y. Xia, ChemSusChem 7 (2014) 1476-1483.

[35] Q. Li, L. Wu, G. Wu, D. Su, H. Lv, S. Zhang, W. Zhu, A. Casimir, H. Zhu, A. Mendoza-Garcia, S. Sun, Nano Lett. 15 (2015) 2468-2473.

[36] R.M. Arán-Ais, F.J. Vidal-Iglesias, J. Solla-Gullon, E. Herrero, J.M. Feliu, Electroanalysis 27 (2015) 945-956.

[37] Y. Garsany, I.L. Singer, K.E. Swider-Lyons, J. Electroanal. Chem. 662 (2011) 396-406.

[38] L. Gan, C. Cui, M. Heggen, F. Dionigi, S. Rudi, P. Strasser, Science 346 (2014) 1502-1506.

[39] C. Cui, L. Gan, M. Heggen, S. Rudi, P. Strasser, Nat. Mater. 12 (2013) 765-771.

[40] D. Alpay, L. Peng, L.D. Marks, J. Phys. Chem. c 119 (2015) 21018-21023.

[41] L.K. Ono, J.R. Croy, H. Heinrich, B. Roldan Cuenya, J. Phys. Chem. C 115 (2011) 16856-16866.

[42] M. Ahmadi, F. Behafarid, C. Cui, P. Strasser, B.R. Cuenya, ACS Nano 7 (2013) 9195-9204.

[43] Y. Hu, P. Wu, Y. Yin, H. Zhang, C. Cai, Appl Catal B-Environ 111–112 (2012) 208-217.

[44] K.-W. Park, J.-H. Choi, B.-K. Kwon, S.-A. Lee, Y.-E. Sung, H.-Y. Ha, S.-A. Hong, H. Kim, A. Wieckowski, J. Phys. Chem. B 106 (2002) 1869-1877.

[45] L.-L. Wang, D.-F. Zhang, L. Guo, Nanoscale 6 (2014) 4635-4641.

[46] T.C. Deivaraj, W. Chen, J.Y. Lee, J. Mater. Chem. 13 (2003) 2555-2560.

[47] F.J. Vidal-Iglesias, R.M. Arán-Ais, J. Solla-Gullon, E. Herrero, J.M. Feliu, ACS Catal. 2 (2012) 901-910.

[48] R.M. Arán-Ais, M.C. Figueiredo, F.J. Vidal-Iglesias, V. Climent, E. Herrero, J.M. Feliu, Electrochim. Acta 58 (2011) 184-192.

[49] R. Rizo, E. Sitta, E. Herrero, V. Climent, J.M. Feliu, Electrochim. Acta 162 (2015) 138-145.

[50] S. Mukerjee, S. Srinivasan, M.P. Soriaga, J. McBreen, J. Phys. Chem. 99 (1995) 4577-4589.

[51] N.M. Markovic, P.N. Ross, Surf. Sci. Rep. 45 (2002) 117-229.

[52] S. Rudi, C. Cui, L. Gan, P. Strasser, Electrocatalysis 5 (2014) 408-418.

[53] M.J.S. Farias, C. Buso-Rogero, R. Gisbert, E. Herrero, J.M. Feliu, J. Phys. Chem. C 118 (2014) 1925-1934.

[54] G. Garcia, M.T.M. Koper, Phys. Chem. Chem. Phys. 10 (2008) 3802-3811.

[55] E. Herrero, Q.-S. Chen, J. Hernandez, S.-G. Sun, J.M. Feliu, Phys. Chem. Chem. Phys. 13 (2011) 16762-16771.

[56] C. Cui, M. Ahmadi, F. Behafarid, L. Gan, M. Neumann, M. Heggen, B.R. Cuenya, P. Strasser, Faraday Discuss. 162 (2013) 91-112.

[57] J. Solla-Gullón, V. Montiel, A. Aldaz, J. Clavilier, J. Electroanal. Chem. 491 (2000) 69-77.

[58] K.J.J. Mayrhofer, M. Hanzlik, M. Arenz, Electrochim. Acta 54 (2009) 5018-5022.

[59] K.J.J. Mayrhofer, V. Juhart, K. Hartl, M. Hanzlik, M. Arenz, Angew. Chem. Int. Ed. 48 (2009) 3529-3531.

[60] M. Ahmadi, C. Cui, H. Mistry, P. Strasser, B. Roldan Cuenya, ACS Nano 9 (2015) 10686-10694.

[61] B. Habibi, E. Dadashpour, Int. J. Hydrogen Energy 38 (2013) 5425-5434.

[62] C.M. Pedersen, M. Escudero-Escribano, A. Velázquez-Palenzuela, L.H. Christensen, I. Chorkendorff, I.E.L. Stephens, Electrochim. Acta 179 (2015) 647-657.

[63] M. Oezaslan, F. Hasché, P. Strasser, J. Electrochem. Soc. 159 (2012) B394-B405.

[64] M. Oezaslan, F. Hasché, P. Strasser, J. Electrochem. Soc. 159 (2012) B444-B454.

[65] C. di Paola, F. Baletto, Phys. Chem. Chem. Phys. 13 (2011) 7701-7707.

[66] R.M. Arán-Ais, Y. Yu, R. Hovden, J. Solla-Gullón, E. Herrero, J.M. Feliu, H.D. Abruña, J. Am. Chem. Soc. 137 (2015) 14992-14998.

[67] M. Oezaslan, P. Strasser, J. Power Sources 196 (2011) 5240-5249.

[68] F. Hasché, M. Oezaslan, P. Strasser, J. Electrochem. Soc. 159 (2012) B24-B33.

[69] F.J. Vidal-Iglesias, J. Solla-Gullón, J.M. Campina, E. Herrero, A. Aldaz, J.M. Feliu, Electrochim. Acta 54 (2009) 4459-4466.

[70] Q.S. Chen, A. Berna, V. Climent, S.G. Sun, J.M. Feliu, Phys. Chem. Chem. Phys. 12 (2010) 11407-11416.

Authors Biography

Rosa M. Arán Ais studied Chemistry (2005-2010) at the University of Alicante and carried out her PhD (2011-2016) at the Institute of Electrochemistry of the same University. As a visiting PhD student, she has collaborated with Prof. Abruña (Cornell University, USA) and Prof. Strasser (TU Berlin, Germany). Her research interests include fundamental and electrocatalytic processes on single crystal electrodes, as well as the synthesis, characterization, and electrocatalytic properties of size- and shape-controlled metal nanoparticles.

Jose Solla Gullón studied at the Universidad de Santiago de Compostela, and carried out his PhD at the Universidad de Alicante (awarded in 2003). Currently, he is senior researcher in the Institute of Electrochemistry at the University of Alicante. Solla Gullón's research is focused on the synthesis, characterization, and electrocatalytic properties of size- and shape-controlled metal nanoparticles.

Marc Heggen is a staff scientist at the Ernst Ruska-Centre, Forschungszentrum Jülich. His main research interests are the microstructural studies on catalysts for energy conversion and storage and the plasticity of structurally complex intermetallic alloys. He obtained his doctorate with Professor K. Urban at the Institute of Microstructural Research. As a visiting scholar he did further research at the Centre d'Ingenierie

des Materiaux, Ecole des Mines, Nancy, France, with Professor Jean-Marie Dubois, and at Harvard School of Engineering and Applied Sciences, Harvard University, Cambridge, MA, USA with Professor Frans Spaepen.

Rafal E. Dunin-Borkowski is Director of the Institute for Microstructure Research and the Ernst Ruska-Centre for Microscopy and Spectroscopy with Electrons in Forschungszentrum Jülich. Between 2007 and 2010, he led the establishment of the Center for Electron Nanoscopy in the Technical University of Denmark. From 2000 to 2006 he held a Royal Society University Research Fellowship in the University of Cambridge. He specializes in advanced transmission electron microscopy. In 2009 he was awarded the Ernst Ruska Prize of the German Society for Electron Microscopy. In 2012 he was awarded an Advanced Grant by the European Research Council.

Peter Strasser is the chaired professor of "Electrochemistry and Electrocatalysis" in the Chemical Engineering Division of the Department of Chemistry at the Technical University Berlin. He was Assistant Professor at the Department of Chemical and Biomolecular Engineering at the University of Houston, after he served as Senior Member of staff at Symyx Technologies, Inc. He earned his PhD in Physical Chemistry and Electrochemistry from the 'Fritz-Haber-Institute' of the Max-Planck-Society in Berlin under the direction of Gerhard Ertl. He studied chemistry at Stanford University, USA, the University of Tuebingen, Germany, and the University of Pisa, Italy. Professor Strasser was awarded the Otto-Roelen medal in Catalysis by the German Catalysis Society, the Ertl Prize, as well as the 'Otto-Hahn Research Medal' by the Max-Planck Society.

Enrique Herrero is professor of Physical Chemistry at the University of Alicante. His research is focuses on electrocatalysis, especially in the reactions involved in fuel cell technologies, trying to understand the fundamental aspects of the reaction mechanisms and how surface structure and composition affect the reactivity. He has published more than 160 peer-reviewed manuscripts in the major journals in the areas of electrochemistry and physical chemistry.

Juan M. Feliu is Professor of Physical Chemistry at the University of Alicante. He obtained his PhD by the University of Barcelona in 1978. His research interests deal with Surface Electrochemistry and Electrocatalysis, aiming to establish relationships between the electrochemical reactivity of metallic electrodes and their surface structure and composition. Juan was Director of the Institute of Electrochemistry of the University of Alicante from 2003 to 2012. He served as President of the International Society of Electrochemistry (2005-2006), is Editor-in Chief of the Journal of Electroanalytical Chemistry and received the Brian E. Conway Prize for Physical Electrochemistry in 2008.

Highlights

- Octahedral PtNi nanoparticles obtained by using the mixture oleylamine/oleic acid as ideal catalysts for the oxygen reduction reaction.
- Critical to the final catalytic activity is the nature of the post synthesis treatment prior to catalyst use.
- Different surface atomic elemental distribution, morphology and composition induced by post-synthesis treatments in vastly different pH environments.
- The composition of the interphase nanoparticle surface/solution can be significantly different from that of the bulk nanocatalyst. Species present at the nanoparticles' surface are pH-dependent, leading to interestingly different catalytic responses.

 In-situ electrochemical measurements like cyclic voltammetry and CO oxidation on a given supporting electrolyte have shown that the modifications prompted under operation conditions are the key to understand the catalyst reactivity.